

Orthogonal calibration via posterior projections with applications to the Schwarzschild model

Antik Chakraborty^{*1}, Jonelle L. Walsh^{†2}, Louis Strigari^{‡2}, Bani K. Mallick^{§3}, and Anirban Bhattacharya^{¶3}

¹Department of Statistics, Purdue University

²George P. and Cynthia Woods Mitchell Institute for Fundamental Physics and Astronomy, Department of Physics and Astronomy, Texas A&M University

³Department of Statistics, Texas A&M University

Abstract

The orbital superposition method originally developed by [Schwarzschild \(1979\)](#) is used to study the dynamics of growth of a black hole and its host galaxy, and has uncovered new relationships between the galaxy's global characteristics. Scientists are specifically interested in finding optimal parameter choices for this model that best match physical measurements along with quantifying the uncertainty of such procedures. This renders a statistical calibration problem with multivariate outcomes. In this article, we develop a Bayesian method for calibration with *multivariate outcomes* using orthogonal bias functions thus ensuring parameter identifiability. Our approach is based on projecting the posterior to an appropriate space which allows the user to choose any nonparametric prior on the bias function(s) instead of having to model it (them) with Gaussian processes. We develop a functional projection approach using the theory of Hilbert spaces. A finite-dimensional analogue of the projection problem is also considered. We illustrate the proposed approach using a BART prior and apply it to calibrate the Schwarzschild model illustrating how a multivariate approach may resolve discrepancies resulting from a univariate calibration.

^{*}antik015@purdue.edu

[†]walsh@physics.tamu.edu

[‡]strigari@tamu.edu

[§]bmалlick@stat.tamu.edu

[¶]anirbanb@stat.tamu.edu

Keywords: Bayesian; Computer model; Emulator; Scientific modeling; Regression trees.

1 Introduction

Scientific endeavors typically aim to describe a natural physical phenomenon. In modern applications, these descriptions increasingly involve complex mathematical equations typically solved using expensive computer codes. For example, the MIT2D climate model (<http://web.mit.edu/globalchange/www/climate.html>) simulates probability distributions of ocean, surface and upper atmospheric temperatures. In our motivating application, Schwarzschild’s orbital integral method (Schwarzschild, 1979) is used to simulate mass distributions of galaxies. These orbit-based models are the main method for measuring the masses of supermassive black holes at the centers of nearby galaxies (Kormendy and Ho, 2013), and have led to the establishment of empirical relationships between the masses of black holes and large-scale galaxy properties, which surprisingly suggest that black holes and their host galaxies grow and evolve together over time (McConnell and Ma, 2013; Kormendy and Ho, 2013; Saglia et al., 2016). Besides determining black hole masses, Schwarzschild modeling is a powerful tool for measuring a galaxy’s mass-to-light ratio, dark matter halo properties, stellar orbital distribution, viewing orientation, and intrinsic three-dimensional shape, allowing for the further study of galaxy assembly histories (Mehrgan et al., 2019). These scientific models involve parameters which carry physical meaning. Inferring about the parameters while addressing the uncertainty of the data observed from the the physical process was first formulated as a statistical problem in Sacks et al. (1989), and was further studied from a Bayesian point of view in Kennedy and O’Hagan (2001), who popularized the term computer code *calibration*. Since then statistical calibration methods have been used in many scientific disciplines; e.g. climatology (Forest et al., 2008; Salter et al., 2018), cell biology (Xie and Xu, 2021), mechanical engineering (Gattiker et al., 2006) etc.

Parallel to the widening applications of statistical calibration methods, substantial effort has also been dedicated to the development of more robust calibration methods within the statistics community, especially after the seminal work of Kennedy and O’Hagan (2001). In their work, the authors proposed a framework that simultaneously models the data observed from a physical process and data generated from computer code implementations of mathematical models emulating the physical process. The fundamental contribution of their work was to include a discrepancy/bias function in their model, which the authors interpreted as a unknown function that captures the inability of the mathematical model to explain variations in the observed data. A Bayesian nonparametric regression approach based on Gaussian processes (Rasmussen and Williams, 2005) was then used to model the unknown bias function as well as the computer code simulating the physical process. This

enabled fast *emulation* of the computer code simulators and produced rapid estimates of input parameters of the computer code that best approximated the observed data. Since then several authors have proposed statistical methods for computer code calibration. [Higdon et al. \(2008\)](#) developed a basis vector approach to calibration when the computer code output is very high-dimensional using principal components; [Bayarri et al. \(2007\)](#) proposed a general framework for Bayesian calibration where a modular Bayes approach was advocated to overcome significant computational and inferential challenges associated with a fully Bayesian analysis of calibration problems; [Chakraborty et al. \(2013\)](#) modeled the computer code using multivariate adaptive regression splines ([Friedman, 1991](#); [Denison et al., 1998](#)) to avoid overfitting the computer model; [Pratola and Higdon \(2016\)](#) proposed to model the bias and computer model using Bayesian additive regression trees (BART; [Chipman et al. \(2010\)](#)) which has gained immense popularity in the machine learning community recently. [Tuo and Wu \(2015, 2016\)](#) studied the general calibration model of [Kennedy and O’Hagan \(2001\)](#) from a theoretical point-of-view and showed that the calibration parameters are not identifiable. As a remedy, [Tuo and Wu \(2015\)](#) defined the calibration parameter as the point in the input parameter space that minimizes the L^2 loss function between the physical process and the computer code. [Plumlee \(2017\)](#) extended it to more general losses and then proposed a modified covariance function for Gaussian process priors used for the bias function; [Xie and Xu \(2021\)](#) treated the calibration parameter as a functional of the bias function and used a projected Bayesian approach to avoid identifiability issues.

In this article, we propose a generalized Bayesian approach for computer code calibration with multivariate output which takes into account identifiability issues pointed out by [Tuo and Wu \(2016\)](#). We start from the definition of the optimal calibration parameter as the point in the input space of the computer code that minimizes a certain loss function. Following [Plumlee \(2017\)](#), this identifiability issue can be mitigated by imposing a orthogonality constraint on the bias function with respect to the derivatives of the computer code. We first generalize the restrictions on the bias function to the situation where there are multiple potentially correlated outcomes. In the univariate outcome case, [Plumlee \(2017\)](#) developed a modified Gaussian process prior on the bias function that respects the orthogonality constraint. However, as indicated by other authors ([Pratola and Higdon, 2016](#)) Gaussian process priors often suffer from scalability issues to big data sets and high-dimensional input spaces. The scalability issues are only exacerbated when one has to deal with multivariate covariance functions. On the other hand, while nonparametric priors such as the BART are highly scalable, introducing a priori constraints such as the orthogonality constraint indicated above is not immediate. To overcome these issues, we propose to posit a unconstrained prior on the bias function and project the obtained posterior on the relevant space. For inference based on the projected posterior we develop two algorithms for posterior sampling. The first one

is essentially a Hilbert projection on the space of square-integrable functions and the second one borrows inspiration from a projection interpretation of the multivariate Gaussian distribution. Numerical experiments in Section 5 show superiority of the proposed method both in terms of computational scalability and modeling flexibility. Indeed, the method provides a more general framework for orthogonal calibration whereby practitioners are free to choose a nonparametric prior of their own choice; for example deep Gaussian process priors used recently in Marmin and Filippone (2022). We also note that our approach is significantly different from a related projection based method by Xie and Xu (2021) where the authors consider a Gaussian process prior on the bias function. The calibration parameter, defined as the minimizer of an appropriate loss function between the observed data and the computer model is then treated as a functional of the bias function. Hence, a prior is induced on the calibration parameter through the Gaussian process prior on the bias function. Although this serves the statistical issue of identifiability, properties of the induced prior is less understood.

The rest of the paper is organized as follows. In Section 2, we briefly describe our motivating example which is then followed by the development of the orthogonal posterior projection approach in Section 3. We then compare the efficiency of the proposed method with other state-of-the-art methods in terms of estimating the calibration parameter and computational scalability. We end with an application on the computer code data from Schwarzschild model. An R package for implementing the proposed method is available to download from <https://github.com/antik015/OCal>.

2 Schwarzschild’s model

The study of the mass distribution within galaxies is central in the quest of understanding of black holes, stellar components, dark matter, and the growth of galaxies. Schwarzschild (1979) presented a orbit superposition method for constructing a self-consistent mass model of galaxies. It consists of “integrating a representative set of orbits in a static triaxial gravitational potential, and finding weights for these orbits such that their superposition reproduces the assumed mass distribution” (Quenneville et al., 2021). Several modifications to the initial method have since been proposed among which van den Bosch et al. (2008)’s triaxial orbit superposition has become very popular. In standard applications of the method, the model is compared with kinematic and photometric data to determine best-fit parameters such as black hole mass (θ_1), stellar mass-to-light ratio (θ_2), and fraction of dark matter halo (θ_2).

In it’s current version (van den Bosch et al., 2008), for a given input parameter combination $t = (t_1, t_2, t_3)^T$, the code outputs the first four moments of the line-of-sight velocity

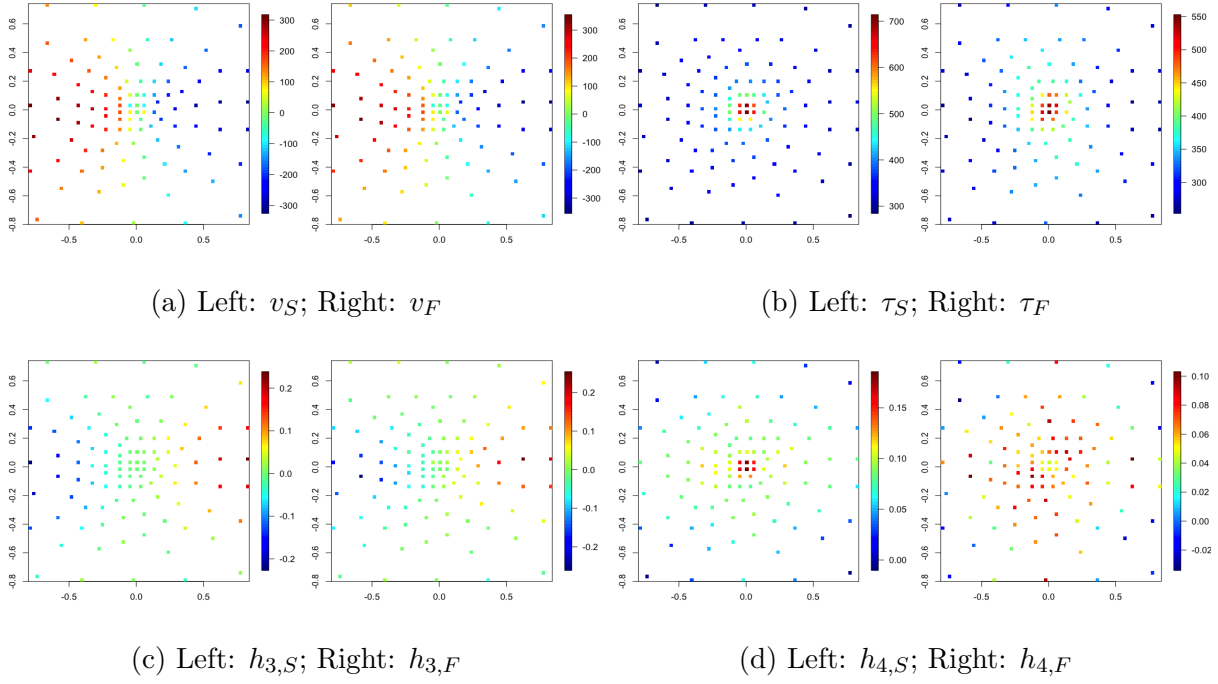


Figure 1: Orbital superposition output versus observed data on four moments of the velocity distribution for $\theta = (10.22, 10, 1)^T$. The superposition method is implemented by a code originally developed by [van den Bosch et al. \(2008\)](#).

distribution $f_S(x; t) = (v_S(x; t), \tau_S(x; t), h_{3,S}(x; t), h_{4,S}(x; t))^T$ for points x in a 2-dimensional spatial grid \mathcal{X} . The points x are typically chosen to match the locations of the physical photometric data, providing further information about the mass distribution. Specifically, physical data $y_F(x_i) = (v_F(x_i), \tau_F(x_i), h_{3,F}(x_i), h_{4,F}(x_i))^T$ is available for $i = 1, \dots, n$, $n = 105$ locations of $\mathcal{X} = [-1, 1]^2$. In Figure 1, color coded output from the code and the observed data are shown when $t = (10.22, 10, 1)^T$ at the n locations. This superposition technique is implemented by a computer code (FORTRAN) which is extremely computationally intensive; e.g. for one input of θ , approximately 3 hours is needed to generate the output. The code output is available for three different values of $t_3 = 1, 2, 3$, and for each value t_3 , the output is available over a two-dimensional grid of values for (t_1, t_2) where t_1 ranges from 10.22 to 10.31 and t_2 ranges from 10 to 10.25. Overall, the computer code output is available for $N = 476$ different values of t . Naturally, an exhaustive search over the input parameter space that compares the code output to the observed data to find the best-fit parameter combination is prohibitive. However, from limited experiments performed separately on each of the 4 outputs of the model, scientists have seen that for the point $\tilde{\theta} = (9.92, 9.29, 1.27)$ the model outputs best approximated the observed data up to slight variations for each of the outcome. It is, however, unclear how a joint analysis of the model outputs and the physical data can be carried out that adequately addresses the uncertainty in the observed data, and whether

such an analysis would reveal regions in the parameter space that perform relatively well. This is important for designing future experiments where scientists plan to include other parameters that could potentially lead to better predictions of the physical process on previously unobserved points - a task typically suited for a multivariate analysis when outcomes are correlated. Inspired by this application, in Section 3, we first develop a general methodology for orthogonal calibration of multivariate computer models where the key focus is on parameter identifiability and modeling flexibility. The validity of the proposed methodology is then investigated in a series of numerical experiments in Section 5, followed by an application on the Schwarzschild’s model in Section 6.

3 Method

3.1 Orthogonal calibration

We begin with a quick review of orthogonal calibration, and introduce notation necessary to develop our method. Suppose we are interested in a real physical system $y_R(\cdot) \in \mathbb{R}^q$, $q \geq 1$ with controllable inputs $x \in \mathcal{X}$ where \mathcal{X} is some closed, bounded subset of \mathbb{R}^d . We do not directly observe the system. Instead, we observe stochastic field observations $y_F(\cdot)$ at n input points called the design $\mathcal{D} = \{x_1, \dots, x_n\}$, for which a natural stochastic model is

$$y_F(x_i) = y_R(x_i) + \epsilon(x_i), \epsilon(x_i) \stackrel{ind.}{\sim} N_q(0, \Sigma_F), i = 1, \dots, n. \quad (1)$$

Suppose in addition to the field observations, we also have a simulator $f : \mathcal{X} \times \Theta \rightarrow \mathbb{R}^q$ for the physical system (depending on the controllable input x as well as other parameters $t \in \Theta \subset \mathbb{R}^p$) which typically comes in the form of a computer code/model. The parameter t represents our understanding of the physical system, and we hope that for some unknown $\theta^* \in \Theta$, the computer model closely approximates the physical process $y_R(\cdot)$. Formally, suppose $L\{y_R(\cdot), f(\cdot, \cdot)\}$ is a loss function that can distinguish between the best possible parameter θ^* and all other parameter values t . If there exists a unique t^* such that $y_R(x) = f(x, t^*)$ for all $x \in \mathcal{X}$ and the loss L is *strictly proper* following Gneiting and Raftery (2007), then $\theta^* = t^*$. However, existence of such a t^* is not always guaranteed for most practical computer models and loss functions. In the absence of such a parameter, the computer model is biased and θ^* is defined as the parameter combination at which the loss $L\{y_R(\cdot), f(\cdot, \cdot)\}$ is minimized, i.e. $\theta^* = \arg \min_{t \in \Theta} L\{y_R(\cdot), f(\cdot, t)\}$. To account for such bias, Kennedy and O’Hagan (2001) proposed the following model for the observed data on the system

$$y_F(x_i) = f(x_i, \theta) + b_\theta(x_i) + \epsilon(x_i), \epsilon(x_i) \stackrel{ind.}{\sim} N(0, \Sigma_F), i = 1, \dots, n, \quad (2)$$

where θ represents the model parameter that targets the population parameter θ^* defined above, and $b_\theta(x)$ is interpreted as the discrepancy or bias between the physical process and the assumed computer model, i.e. $b_\theta(x) = y_R(x) - f(x, \theta)$. Without added restrictions in (2), θ is not identifiable in (2). We provide a sufficient condition for identifiability under the loss

$$L\{y_R(\cdot), f(\cdot, t)\} = \sum_{k=1}^q \int_{\mathcal{X}} \{y_{R,k}(x) - f_k(x, t)\}^2 dx, \quad (3)$$

in the following proposition, extending the result of Plumlee (2017) to multivariate outcomes.

Proposition 3.1. *Consider the loss $L\{y_R(\cdot), f(\cdot, t)\}$ defined above. Let $g_{j,k}(x, t) = \frac{\partial}{\partial t_j} f_k(x, t)$, the partial derivative with respect to t_j of the k -th component $f_k(x, t)$ of the computer model $f(x, t)$, which is assumed to exist for all j, k . A sufficient condition for $\frac{\partial}{\partial t} L\{y_R(\cdot), f(\cdot, t)\}|_{t=\theta^*} = 0$ is*

$$\int_{\mathcal{X}} \sum_{k=1}^q g_{j,k}(x, \theta^*) b_{\theta^*,k}(x) dx = 0, \quad \text{for all } j = 1, \dots, p. \quad (4)$$

Proof. Write $y_{R,k}(x) = f_{k,\theta}(x) + b_{\theta,k}(x)$ to obtain that the j -th element of

$$\frac{\partial}{\partial t} L\{y_R(\cdot), f(\cdot, t)\}|_{t=\theta} = -2 \int_{\mathcal{X}} \sum_{k=1}^q g_{j,k}(x) b_{\theta,k}(x) dx,$$

and recall $\theta^* = \arg \min_{t \in \Theta} L\{y_R(\cdot), f(\cdot, t)\}$ which completes the proof. \square

In other words, if the bias functions satisfy a linear constraint with respect to the gradients of the computer model at θ , then θ is identifiable.

3.2 Bayesian inference on model (2)

The influential paper Kennedy and O'Hagan (2001) originally proposed the model (2) for $q = 1$, and considered Gaussian process priors (Rasmussen and Williams, 2005) as a prior distribution over the unknown function $b_\theta(x)$ together with a Normal/Uniform prior over the parameter θ . For now, we assume that the functional form of the computer model $f(x, t)$ is explicitly known for every $x \in \mathcal{X}, t \in \Theta$ and defer the extension of the proposed method to unavailable f later. A Gaussian process prior over an unknown function $h(\cdot)$ is typically elicited by a mean function $m(\cdot)$ and a covariance function $C(\cdot, \cdot)$. Under this prior, for any finite collection of points $\{u_1, \dots, u_N\}$, the prior distribution over the vector $\{h(u_1), \dots, h(u_N)\}^T$ has a multivariate Gaussian distribution with mean $\{m(u_1), \dots, m(u_N)\}$ and covariance matrix $K = (K_{ij})$ and $K_{ij} = C(u_i, u_j)$, $1 \leq i, j \leq N$. Let $\Pi(\theta)$ be the prior distribution over θ and suppose b_θ is endowed with a Gaussian process prior with a zero mean function and a covariance kernel $C(\cdot, \cdot)$. Then with n observations on $y_F(\cdot)$ on the design \mathcal{D} ,

the posterior distribution of (θ, \mathbf{b}) , $\mathbf{b} = \{b_\theta(x_1), \dots, b_\theta(x_n)\}^\top$ can be obtained using Bayes theorem as

$$\Pi(\theta, \mathbf{b} \mid y^{(n)}) \propto \ell(y^{(n)} \mid \theta, \mathbf{b})\Pi(\theta)\Pi(\mathbf{b}), \quad (5)$$

where given θ , $y^{(n)} = \{y_F(x_1) - f(x_1, \theta), \dots, y_F(x_n) - f(x_n, \theta)\}^\top$ and $\ell(y^{(n)} \mid \theta, \mathbf{b})$ is the likelihood corresponding to a Gaussian distribution with mean \mathbf{b} and covariance matrix $\sigma_F^2 \mathbf{I}_n$. The marginal posterior distribution of θ , $\Pi(\theta \mid y^{(n)})$ can be obtained by observing that $y^{(n)} \mid \theta \sim \mathcal{N}(0, K + \sigma_F^2 \mathbf{I}_n)$.

Tuo and Wu (2016) proved that vanilla Gaussian process priors over the bias $b_\theta(\cdot)$ may lead to inaccurate inference on θ^* , defined as the minimizer of the loss function discussed above, even when observations are available for a large number of points n . This is mainly due to the fact that a generic Gaussian process on the bias function is not guaranteed to satisfy the orthogonality condition (4). In light of this, Plumlee (2017) advocated a modified covariance kernel for $b_\theta(\cdot)$ such that realizations of such a Gaussian process prior satisfy (4) almost surely, see also Plumlee and Joseph (2018). This modified covariance kernel is

$$C_\theta(x, x') = C(x, x') - h_\theta(x)^\top H_\theta^{-1} h_\theta(x'), \quad (6)$$

where the j -th element of the vector $h_\theta(x) \in \mathbb{R}^p$ is given by $\int_{\mathcal{X}} g_j(x, \theta) C(x, u) du$ and the (j, k) -th element of the matrix $H_{\theta_0} \in \mathbb{R}^{p \times p}$ is $\int_{\mathcal{X}} \int_{\mathcal{X}} g_j(u, \theta) g_k(u', \theta) C(u, u') du du'$ with $x, x' \in \mathcal{X}$ for $1 \leq j, k \leq p$. This covariance function is obtained by observing that under a Gaussian process prior on b_{θ_0} , the prior on $(b_\theta, \int_{\mathcal{X}} g_1(x, \theta) b_\theta(x) dx, \dots, \int_{\mathcal{X}} g_p(x, \theta) b_\theta(x) dx)$ is again a Gaussian process and one then simply finds the conditional covariance of b_θ given that the last p elements of the above vector are 0, and thus the orthogonality condition in (4) is enforced. Of course, apriori we do not have knowledge on θ . However, assuming the knowledge of the system $y_R(x)$ and the computer model $f(x, t)$ for all $t \in \Theta$, a consistent estimator of θ can be used for implementing orthogonal covariance function in practice (Plumlee, 2017).

3.3 Posterior projections

Although the modified covariance kernel seemingly resolves identifiability issue of θ , it hinges on the assumption that the user chooses to model $b_\theta(x)$ with a Gaussian process. This leaves out a plethora of other nonparametric priors for functions that have been widely popular in the literature, for example Bayesian additive regression trees (BART) (Chipman et al., 2010), Bayesian multivariate adaptive regression splines (Denison et al., 1998), Bayesian neural networks (Neal, 2012) etc. Furthermore, these methods have been successfully applied in computer code calibration problems (Pratola and Higdon, 2016; Higdon et al., 2008; Chakraborty et al., 2013). Many of these priors have been shown to have optimal theoretical

properties along with sufficient computational scalability (Ročková and van der Pas, 2020; Linero and Yang, 2018). In this article, our aim is to develop a procedure where a user is free to choose any nonparametric prior for $b_\theta(x)$ and the procedure automatically takes care of orthogonality constraints discussed above.

Let $L_q^2(\mathcal{X})$ be the space of q -dimensional square-integrable functions on \mathcal{X} equipped with the inner-product $\langle f_1, f_2 \rangle = \sum_{k=1}^q \int f_{1,k}(x) f_{2,k}(x) dx$. Then $L_q^2(\mathcal{X})$ is a tensor Hilbert space with norm $\|\cdot\|_{L_q^2}$ induced by the inner product: $\|f\|_{L_q^2} = \langle f, f \rangle = \sum_{k=1}^q \int f_k^2(x) dx$. We assume that for every $t \in \Theta$, $g_j(\cdot, t) = (g_{j,1}(\cdot, t), \dots, g_{j,q}(\cdot, t))^T \in L_q^2(\mathcal{X})$ for all $j = 1, \dots, p$ and the corresponding bias $b_t(\cdot) \in L_q^2(\mathcal{X})$. Define $\mathcal{F}_{\tilde{\theta}} = \{b_{\tilde{\theta}} : \int \sum_{k=1}^q g_{j,k}(x, \tilde{\theta}) b_{\tilde{\theta},k}(x) dx = 0, j = 1, \dots, p\}$ for a fixed $\tilde{\theta}$. Here $\tilde{\theta}$ is our guess about the parameter combination at which the computer model best approximates the system given the observed data and the computer model. Such a data-dependent choice of $\tilde{\theta}$ involves minimizing the corresponding empirical risk. Let $\tilde{\theta}$ be defined as

$$\tilde{\theta} = \arg \min_{t \in \Theta} \frac{1}{nq} \sum_{k=1}^q \sum_{i=1}^n \{y_{F,k}(x_i) - f_k(x_i, t)\}^2. \quad (7)$$

Validity of this definition is provided in the following result where we first establish θ^* as the minimizer of population risk and then leverage on empirical risk minimization results to show that $\tilde{\theta}$ converges to θ^* for large n .

Proposition 3.2. *Let $P = P_{y|x}P_x$ denote the data generating distribution where P_x is the uniform measure on \mathcal{X} . Suppose that Θ is compact and that the k -th computer model is Lipschitz in $t \in \Theta$ uniformly over $x \in \mathcal{X}$, that is there exists $L_k > 0$ such that $|f_k(x, t_1) - f_k(x, t_2)| \leq L_k \|t_1 - t_2\|_2^2$ for $k = 1, \dots, q$. Then $\tilde{\theta} \xrightarrow{P} \theta^*$.*

A proof is provided in the appendix. Our definition of $\tilde{\theta}$ is different from the definition used in (Plumlee, 2017, Proposition 1) where the author assumes the knowledge of $y_R(\cdot)$ along with the computer model $f(\cdot, t)$ for all t . We argue that explicit functional form of $y_R(\cdot)$ may not be available in many practical scenarios, and hence define $\tilde{\theta}$ as detailed above. The compactness of Θ is a technical assumption which nevertheless is often practical in many calibration problems.

Having defined the point at which we want the bias function $b(x)$ to satisfy the orthogonality condition (4), we now proceed to define the projection posterior. Instead of defining a prior distribution on $b_{\tilde{\theta}} \in \mathcal{F}_{\tilde{\theta}}$, our strategy is to start with a generic prior and then project the posterior distribution to $\mathcal{F}_{\tilde{\theta}}$. Standard Hilbert space theory implies that $\mathcal{F}_{\tilde{\theta}}$ is a non-empty, closed and convex subset of $L_q^2(\mathcal{X})$. Then by the Hilbert projection theorem (Tsiatis,

2006), there exists a unique projection b_θ^* of any $b_\theta \in L_q^2(\mathcal{X})$. Define the projection as

$$T_{\mathcal{F}_\theta}(b_\theta) = \{b_\theta^* \in \mathcal{F}_\theta : \|b_\theta^* - b_\theta\|_{L_q^2} = \inf_{b \in \mathcal{F}_\theta} \|b - b_\theta\|_{L_q^2}\}. \quad (8)$$

We now describe how $T_{\mathcal{F}_\theta}$ is used to define the projection posterior. Suppose a prior distribution $\Pi(\theta, b) = \Pi(\theta)\Pi(b)$ is elicited on $\Theta \times L_q^2(\mathcal{X})$. Let $\tilde{B} = \tilde{B}_1 \times \tilde{B}_2$ be a measurable subset of the Borel σ -algebra of $\Theta \times \mathcal{F}_\theta$. Then given $y^{(n)}$, we define the posterior probability $\Pi_{\text{proj}}(\tilde{B} \mid y^{(n)})$ of \tilde{B} under the prior $\Pi(\theta, b)$ as $\Pi(B \mid y^{(n)})$ where $B = \tilde{B}_1 \times T_{\mathcal{F}_\theta}^{-1}(\tilde{B}_2)$ where $T_{\mathcal{F}_\theta}^{-1}(\tilde{B}_2) = \{b_\theta : T_{\mathcal{F}_\theta}(b_\theta) \in \tilde{B}_2\}$, that is,

$$\Pi_{\text{proj}}(\tilde{B} \mid y^{(n)}) = \Pi(B \mid y^{(n)}) = \frac{\int_B \ell(y^{(n)} \mid \theta, b) d\Pi(\theta, b)}{\int \ell(y^{(n)} \mid \theta, b) d\Pi(\theta, b)}. \quad (9)$$

Measurability of T is guaranteed since \mathcal{F}_θ is non-empty, closed and convex; see also [Sen et al. \(2018\)](#). Although (8) is defined as a solution to an optimization problem, in this particular case, it has an explicit form which we call functional projection.

Lemma 3.3. *Fix $b \in L_q^2(\mathcal{X})$ and let $\tilde{\theta}$ be defined as above. Let the functions $g_{j,k}(x)$, $j = 1, \dots, p$ satisfy the following: $\sum_{j=1}^p \alpha_j g_{j,k}(x) = 0$ for all $x \in \mathcal{X}$ and for all $k = 1, \dots, q$ iff $\alpha_j = 0$, $j = 1, \dots, p$. Then $T_{\mathcal{F}_\theta}(b) = b^*(x) = b(x) - \sum_{j=1}^p \lambda_j^* g_j(x)$ where the vector $\lambda = (\lambda_1^*, \dots, \lambda_p^*)^T$ satisfies $Q\lambda = \eta$ with $\eta = (\sum_{k=1}^q \langle b_k, g_{1,k} \rangle, \dots, \sum_{k=1}^q \langle b_k, g_{p,k} \rangle)^T$ and Q is a $p \times p$ matrix with elements $Q_{jj'} = \sum_{k=1}^q \langle g_{j,k}, g_{j',k} \rangle$.*

The proof is provided in the Appendix. Having defined the projection for our purpose, we can then devise an MCMC algorithm to sample from $\Pi_{\text{proj}}(\cdot \mid y^{(n)})$ defined in (9).

Algorithm 1: Projection sampler 1

1. Update $b_\theta \sim \Pi(b_\theta \mid \theta, y^{(n)})$
 2. Project b_θ onto \mathcal{F}_θ following the Proposition 3.3 to obtain b_θ^* .
 3. Update $\theta \sim \Pi(\theta \mid b_\theta^*, y^{(n)})$.
-

As an example, consider the case when b_θ is endowed with a zero mean Gaussian process prior with covariance kernel $C(\cdot, \cdot)$. Then following Algorithm 1, we update $b_\theta \sim \Pi(b \mid \tilde{\theta}, y^{(n)})$ which is a multivariate Gaussian distribution. Next, we compute the corresponding projection b_θ^* using Lemma 3.3. Finally, we sample $\theta \sim \Pi(\theta \mid b_\theta^*, y^{(n)})$. This strategy also works for other priors such as BART, where in the first step we update the parameters of the BART parameters using their respective full conditionals. The next steps are exactly the same. An alternative finite-dimensional projection method is described in the supplementary document.

For a full Bayesian inference on (2) under the projection posterior framework described above, one should ideally elicit a prior $\Pi(\Sigma_F)$ on the unknown covariance matrix Σ_F . However, this often adds to computational challenges already present in a calibration problem and may not influence the uncertainty observed in θ - the central goal of these problems (Bayarri et al., 2007). As an alternative, a modular Bayes approach is considered here where we use a plug-in estimate $\hat{\Sigma}_F$. This estimate is constructed by fitting a nonparametric regression model, i.e. $y_{F,k}(x) = y_{R,k}(x) + \epsilon_k(x)$ to each outcome separately with idiosyncratic variance parameters $\sigma_{F,k}^2$ with conjugate Inverse Gamma priors and $y_{R,k} \sim \Pi_k$ for some nonparametric prior on $y_{R,k}$. We then set $\hat{\Sigma}_F = \text{Cov}(E)$ where E is the error matrix with columns $E_k = y_{F,k} - \bar{y}_R$ where \bar{y}_R is the posterior mean of predictions on the training set. Given $\hat{\Sigma}_F$, it can be assumed without loss of generality that $\epsilon(x) \sim N(0, I_q)$ in (2). This also makes prior elicitation on the multivariate bias b simpler; a natural choice is $\Pi(b) = \prod_{k=1}^q \Pi(b_k)$.

4 Explicitly unavailable computer model

Until now we have assumed that the computer model $f(x, t)$ is either explicitly specified or can be evaluated cheaply using a code for every $(x, t) \in \mathcal{X} \times \Theta$. However, in many calibration problems, including ours, this is not the case; the computer code can be computationally very expensive; see also Section 2. The standard approach in the literature has been to approximate the computer model using a nonparametric method, typically the Gaussian process (Santner et al., 2003). While the original calibration framework developed by Kennedy and O’Hagan (2001) modeled the observed data and the computer model simultaneously, a modular approach to inference has been advocated by many authors, e.g. Bayarri et al. (2007); Plumlee (2017) wherein the modeling of the explicitly defined computer model is done separately from the modeling of the observed data. Here, we adopt this modular approach with one crucial difference with Plumlee (2017) where the author uses a probabilistic definition of the computer model using a Gaussian process. We, on the other hand, use a deterministic definition \hat{f} of the computer model obtained using any nonparametric approximator such as the posterior mean of a BART fit, a neural net obtained by minimizing the least square error between code evaluations and the neural net output, or a random forest fit; such an approach was also adopted by Xie and Xu (2021). Our motivation for doing so is to allow for more computational and modeling flexibility than a Gaussian process framework. Specifically, we work with the posterior mean of a BART fit which proved to be superior among all other choices of models for $f(x, t)$ in our numerical experiments as well as in our motivating example. In particular, we compared the squared error loss on a held-out test data of size $n_t = 50$ for these methods: $(n_t)^{-1} \sum_{i=1}^{n_t} \{f(x, t_i) - \hat{f}(x, t_i)\}^2$ for each location x in the observed data $x \in \mathcal{X}$ and each output of the computer model. In the best case

scenario, the ratio of the squared error loss for the posterior predictive mean improved over the second best method (Random Forest) by a factor of almost 5.

5 Simulations and univariate applications

5.1 Univariate simulations

In this section, we compare our method to the GP orthogonal calibration by Plumlee (2017) (OGP) and the projected calibration (PCAL) method by Xie and Xu (2021) in several simulation experiments. Since these methods were originally developed for one outcome, we restrict here to the case $q = 1$. We focus on each of these methods' ability to estimate θ^* , uncertainty quantification, and their associated computing time. For generating the data, we consider two situations when the definition of the computer model is available explicitly:

1. **Model 1:** $y_R(x) = 4x + x \sin 5x$, $f(x, t) = tx$ where $x \in [0, 1]$ (Plumlee, 2017, Example 5.1),
2. **Model 2:** $f(x, t) = 7\{\sin(2\pi t_1 - \pi)\}^2 + 2\{(2\pi t_2 - \pi)^2 \sin(2\pi x - \pi)\}$, $y_R(x) = f(x, \theta^*)$ where $\theta^* = (0.2, 0.3)$, $x \in [0, 1]$ (Xie and Xu, 2021, Configuration 1).

In **Model 1**, $\theta^* = 3.56$. We additionally consider one more situation where we do not assume the knowledge of $f(x, t)$ in **Model 2** and approximate it by the posterior predictive mean of a BART when $N = 7^2$ code outputs are available on the observed values of x , meaning we have for each value $\{\theta_1, \dots, \theta_N\}$ the computer code output is available for $f(\theta_k, x_i)$, $k = 1, \dots, N, i = 1, \dots, n$.

- **Model 3:** $f(x, t)$ is same as **Model 2** but only outputs f_1, \dots, f_N are available. Everything else is same as **Model 2**.

In this case, we set $\tilde{\theta}$ to be the parameter value at which the sample L^2 -distance is minimized between the observed data and the posterior predictive mean of f .

For all cases we simulate $n = 100$ field observations from the model $y^F(x_i) = y^R(x_i) + \epsilon_i$, $\epsilon_i \sim N(0, 0.2^2)$ where we sample the x_i 's uniformly over $[0, 1]$. For the proposed method, we consider two priors on the bias function - GP and BART. For the GP prior, we use the covariance kernel $C(x, x') = \sigma^2(1 + |x - x'|/\psi) \exp\{-|x - x'|/\psi\}$. We set $\psi = 1/2$ and use a plug-in estimate of σ^2 which is obtained by fitting a non-parametric BART regression model to the observed field data $(y_{F,i}, x_i)_{i=1}^n$. The corresponding projected versions are abbreviated as PGP and PBART. We also consider the functional and finite dimensional projections for PGP and PBART, with the finite-dimensional version abbreviated as PGP(Fn) and PBART(Fn). For Model 3, we only consider the infinite dimensional projections. In Tables

Model 1 ($\theta^* = 3.56$)						
	PGP	PGP(Fn)	PBART	PBART(Fn)	OGP	PCAL
Mean	3.56	3.59	3.57	3.58	3.57	3.57
Std. Dev.	0.008	0.007	0.02	0.02	0.003	0.003
Coverage	0.93	0.93	0.92	0.93	0.95	0.95
Runtime	3.78 sec	30.72 sec	1.86 sec	17 min	1.88	13.92 min

Table 1: Simulation results for **Model 1**. We report the posterior mean, posterior standard deviation, coverage of the 95% credible intervals and the average runtime.

Model 2 ($\theta^* = (0.2, 0.3)$)						
	PGP	PGP(Fn)	PBART	PBART(Fn)	OGP	PCAL
Mean	(0.2, 0.3)	(0.2, 0.31)	(0.19, 0.3)	(0.2, 0.31)	(0.2, 0.3)	(0.2, 0.3)
Std. Dev.	(0.0002, 0.0002)	(0.0003, 0.0004)	(0.0008, 0.0007)	(0.0008, 0.0008)	(0.001, 0.002)	(0.003, 0.0006)
Coverage	0.91	0.91	0.92	0.92	0.96	0.96
Runtime	18.18 sec	2.65 min	9.38 sec	1.35 hrs	16.58 min	

Table 2: Simulation results for **Model 2**. We report the posterior mean, posterior variance, coverage of the 95% credible intervals and the average runtime.

1, 2 and 3 we report the results of our experiments from a replicated simulation study. All numbers are averaged over 100 replications and for each model we draw 5000 posterior samples using MCMC with 1000 burn in samples. In terms of estimation quality of the calibration parameters, all the different methods perform similarly. Indeed, the posterior mean and standard deviation in Table 1 and Table 2 are almost identical. However, the key difference is in the respective runtimes of these methods. The runtimes reported in the tables are comparable up to coding language and efficiencies of these implementations. Nonetheless, PBART outperforms all other methods by quite a large margin providing at least an order of magnitude improvement over the next fastest method. We note here, the runtimes reported for PCAL correspond to the standard implementation of the method and not the approximated calibration method proposed in Xie and Xu (2021); the approximated calibration method is much faster compared to its standard version although even for that the average runtime for **Model 2** is 36.33 seconds which is almost 4 times the time of PBART. In terms of uncertainty quantification, all the methods in consideration provide roughly the nominal coverage although it seems that PGP and PBART is biased downwards (but only slightly). This is also apparent in the relatively sharper posterior distributions of θ plotted in Figure 2.

5.2 Univariate analysis on Schwarzschild model outputs

We apply the proposed posterior projection technique on each output of the Schwarzschild model separately. We illustrate the specifics of our application with the first output of the Schwarzschild model, which is the mean velocity. Similar to the Kennedy and O’Hagan

Model 3 ($\theta_0 = (0.2, 0.3)$)		
	PGP	PBART
Mean	(0.21, 0.33)	(0.22, 0.34)
Std. Dev.	(0.03, 0.03)	(0.04, 0.03)
Runtime	24 min	20 min

Table 3: Simulation results for **Model 3**. We report the posterior mean, posterior variance and the average runtime.

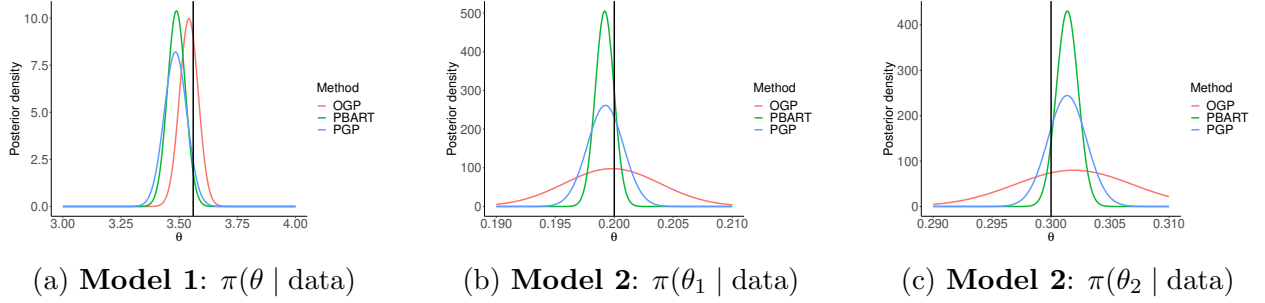


Figure 2: Posterior distribution of the calibration parameter θ .

(2001) setup, we have the following model for the observed velocities $v_F(x)$ and the corresponding code output $v_S(x)$ at location $x \in \mathcal{X}$:

$$v_F(x_i) = v_R(x_i) + \epsilon_i = v_S(x_i; \tilde{\theta}) + b_{v, \tilde{\theta}}(x_i) + \epsilon_i, \quad \epsilon_i \sim \mathcal{N}(0, \sigma_v^2), \quad (10)$$

where we let $\tilde{\theta}$ to be the parameter value where the L^2 loss defined in previous sections is minimized and $b_{v, \tilde{\theta}}(\cdot)$ is the bias function corresponding to mean velocity at $\tilde{\theta}$. Since the explicit form of the model is not available, we use the posterior mean of a BART fit as the definition of $v_S(x; t)$ based on the model outputs only. We fix σ_v to the posterior mean of σ of a BART regression fit to $(v_{F,i}, x_i)_{i=1}^n$. We set $\theta_j \sim \mathcal{N}(0, \gamma^2)$ with $\gamma = 10$ as priors for θ_j , and $\Pi(\theta) = \prod_{j=1}^p \Pi(\theta_j)$. We implement PGP and PBART under these settings where for implementing Step 3 of Algorithm 1, we use an adaptive Metropolis-Hastings sampler Haario et al. (2001) which is tuned to maintain an acceptance rate of approximately 0.3.

In Table 4, we summarize the posterior distribution of the calibration parameters for all the four different outputs of the Schwarzschild model. Specifically, we report the posterior mean, standard deviation and the 95% credible interval for all the three calibration parameters $(\theta_1, \theta_2, \theta_3)$. As expected, there are some differences in the posterior means for different velocity moments being fit. For example, the posterior mean for θ_1 differs when using h_4 compared to when using τ . The difference may be due to the physical degeneracy between the orbital anisotropy and black hole mass, such that large τ at the center of the 2-dimensional spatial grid can imply a large black hole mass but so too can a smaller τ with radial anisotropy, which is reflected in the values of h_4 . Or, it could be due simply to the

		PGP			PBART		
		θ_1	θ_2	θ_3	θ_1	θ_2	θ_3
v	Mean	9.46	9.06	0.82	9.59	9.16	1.22
	Std. Dev.	0.14	0.08	0.09	0.27	0.15	0.07
	Interval	(9.21, 9.80)	(8.93, 9.18)	(0.65, 1.00)	(9.20, 9.97)	(8.93, 9.50)	(1.12, 1.32)
τ	Mean	9.98	9.12	1.02	9.59	9.03	1.42
	Std. Dev.	0.09	0.07	0.10	0.10	0.13	0.18
	Interval	(9.81, 10.14)	(8.99, 9.26)	(0.87, 1.23)	(9.41, 9.76)	(8.84, 9.31)	(1.15, 1.76)
h_3	Mean	9.96	9.36	1.04	10.09	9.27	1.41
	Std. Dev.	0.07	0.08	0.12	0.07	0.08	0.06
	Interval	(9.86, 10.11)	(9.15, 9.49)	(0.87, 1.25)	(9.97, 10.23)	(9.12, 9.41)	(1.25, 1.41)
h_4	Mean	10.18	9.07	1.09	9.73	9.09	1.53
	Std. Dev.	0.11	0.06	0.06	0.06	0.12	0.09
	Interval	(9.89, 10.62)	(8.97, 9.20)	(0.97, 1.19)	(9.61, 9.82)	(8.85, 9.28)	(1.35, 1.69)

Table 4: Posterior summaries for the calibration parameters θ_1 = logarithm of mass of the black hole, θ_2 = stellar mass-to-light ratio and θ_3 = fraction of dark matter. The posterior mean, standard deviation (Std. Dev.) and the 95% credible interval is reported here.

model inadequacy of a univariate treatment of the problem. In addition, there seems to a broad agreement between the posterior means for θ_1 and θ_2 under the two priors. However, the key difference is in the posterior mean of θ_3 . For the GP prior, the posterior mean for the 4 outcomes is roughly around 1, whereas for BART, the posterior mean is around 1.4. One possible explanation for this discrepancy is that for θ_3 , the computer code output is only available for $\theta_3 = 1, 2, 3$. The scarcity of data along this dimension may potentially lead to unstable estimates. A joint model accounting for the covariance between the measurements can reconcile this apparent discrepancy in the posterior distribution and the problems induced by sparse data. Numerical experiments in the next subsection illustrates the benefits of a joint model when outcomes are correlated.

5.3 Multivariate simulations

Here we consider a simulation scenario where more than outcome is measured, i.e. $q > 1$. We illustrate this with the case $q = 2$. For $x \in [0, 1]$, consider the model

$$\begin{pmatrix} y_{F,1}(x) \\ y_{F,2}(x) \end{pmatrix} = \begin{pmatrix} f_1(x, \theta) \\ f_2(x, \theta) \end{pmatrix} + \begin{pmatrix} b_{\theta,1}(x) \\ b_{\theta,2}(x) \end{pmatrix} + \begin{pmatrix} \epsilon_1 \\ \epsilon_2 \end{pmatrix} \quad (11)$$

where $y_{R,1}(x) = 4x + x \sin 5x$, $y_{R,2}(x) = [1 + \exp\{-6(x - 0.5)\}]^{-1}$ are the real data-generating processes. The respective computer models are $f_1(x, t) = tx$, $f_2(x, t) = \Phi\{t(x - 0.5)\}$ with $\Phi(\cdot)$ being the cdf of $Z \sim N(0, 1)$. The errors are assumed to follow $N(0, \Sigma)$. The loss $L\{y_R(\cdot), f(\cdot, t)\} = \sum_{k=1}^2 \int_{\mathcal{X}} \{y_{R,k}(x) - f_k(x, t)\}^2$ is minimized at $\theta^* = 3.56$ approximately. However, the behavior of the L_2 -loss in these two cases is very different, especially near the

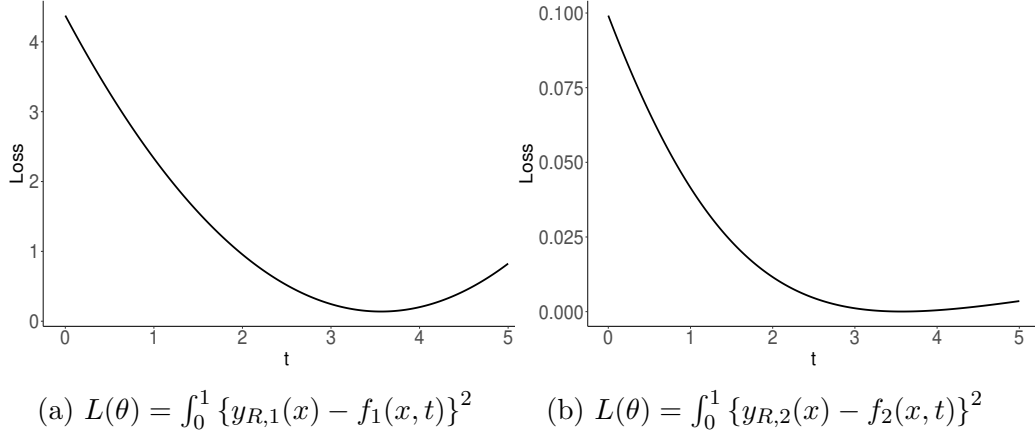


Figure 3: Loss comparison

minimum. Indeed, as shown in the left panel of Figure 3, for the pair $(y_{R,1}, f_1)$, the loss increases quite sharply around 3.56, whereas for $(y_{R,2}, f_2)$, the increase in loss for $t > 3.56$ is much slower. As such, when data from model (11) is fitted separately in the univariate framework, one should expect more uncertainty in θ for $(y_{R,2}, f_2)$. On the other hand, a joint multivariate fit should reflect the fact when the two real processes and their corresponding computer models are compared together, the posterior distribution of θ is much more centered around 3.56.

For data generation, we consider $n = 100$ and a covariance matrix Σ_0 such that the diagonal elements are 0.2^2 and the off-diagonal elements are 0.012. We consider PGP and PBART for this setup and use the functional projection. We fit this data separately in the univariate framework and then a joint model is fitted. For a fair comparison all hyperparameter values were the same. We plot the posterior distribution of θ obtained using the PBART method in Figure 4. In the first and second panel, the posterior distribution of θ is shown when two separate univariate models are fitted, and in the third panel we show that for a multivariate fit. As mentioned earlier, the posterior distribution of θ when data for the second outcome is fitted separately, is more dispersed and has relatively large mass in the interval $[3, 4]$. This is not the case for the first outcome, as almost the entire mass is within $[3.5, 3.65]$. However, the posterior distribution of θ from a multivariate fit is able to borrow information across the two outcomes so that most of the mass of the distribution is within $[3.4, 3.7]$.

6 Calibrating the Schwarzschild model

Here we carry out a joint calibration of the Schwarzschild model. For this, we first estimate the covariance matrix as $\Sigma = \text{Cov}(E)$, where E is a $n \times q$ error matrix obtained by fitting

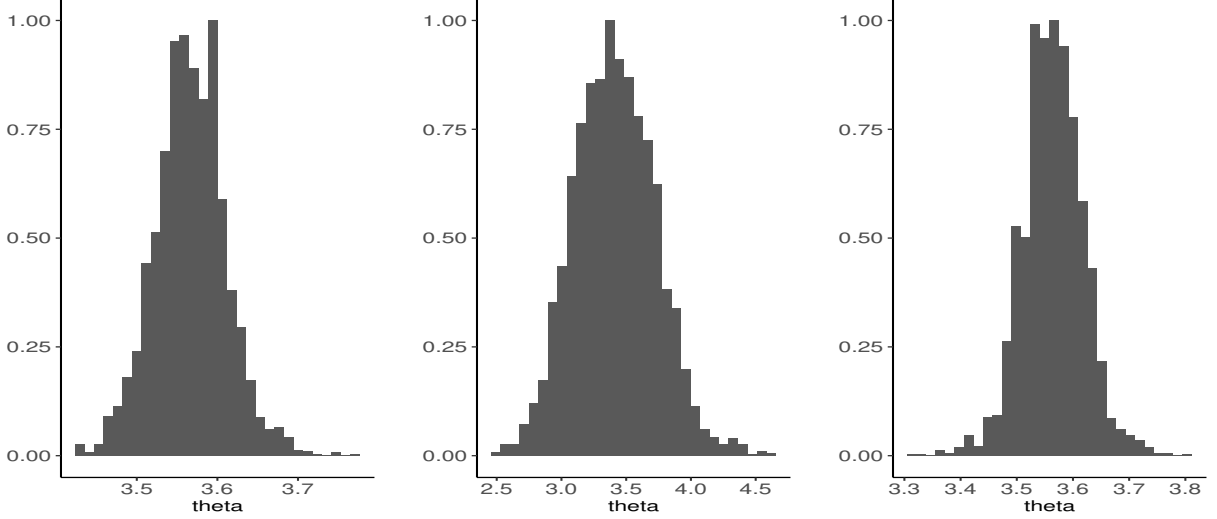


Figure 4: Posterior distribution of θ for univariate and multivariate PBART fits for model 11. Left two panels show posteriors for two separate univariate fits, and the third panel shows posterior from a combined multivariate fit.

univariate BART regressions to the field data of each outcome. Here we fit the PBART method with functional projection. The marginal posterior distribution of θ is shown in Figure 5. The 95% symmetric posterior (marginal) credible intervals are [9.54, 9.87], [8.78, 9.13] and [0.97, 1.38] for $\theta_1, \theta_2, \theta_3$, respectively. Intervals for θ_1, θ_2 from the joint analysis clearly seem to lie at the intersection of the intervals from the univariate model, but the posterior of θ_3 exhibits slight bimodality. Overall, by modeling the four outcomes simultaneously uncertainty in θ have reduced which may significantly cut down computation time for future applications with an expanded parameter space. We also show the marginal posterior predictive mean of the outcomes. In the first panel of Figure 6, we plot the posterior predictive mean at the observed locations for $v_R(\cdot)$. For reference, the observed data is plotted on the third panel of Figure 6. Similar plots for $\tau_R(\cdot), h_{3,R}(\cdot)$ and $h_{4,R}(\cdot)$ are provided in Figures 7, 8 and 9, respectively. As mentioned earlier, the outcomes in this context represent the first four moments of velocity, and the model performance decreases as the moments increase. We also observed a similar phenomenon when we looked at the relative squared error loss for a held-out data set of size 20. For $v_F(x)$, We define the relative squared error loss as $n_t^{-1} \sum_{i=1}^{n_t} (1 - \hat{v}_F(x_i)/v_F(x_i))^2$ where $\hat{v}_F(x_i)$ represents the posterior mean of samples of $[v_S(x_i, \theta) + b_{v,\theta}(x_i)]$. Here n_t is the test data size. The definition is similar for other outcomes. The values we obtained are 0.17, 0.003, 3.92 and 30.42 for v, τ, h_3, h_4 , respectively.

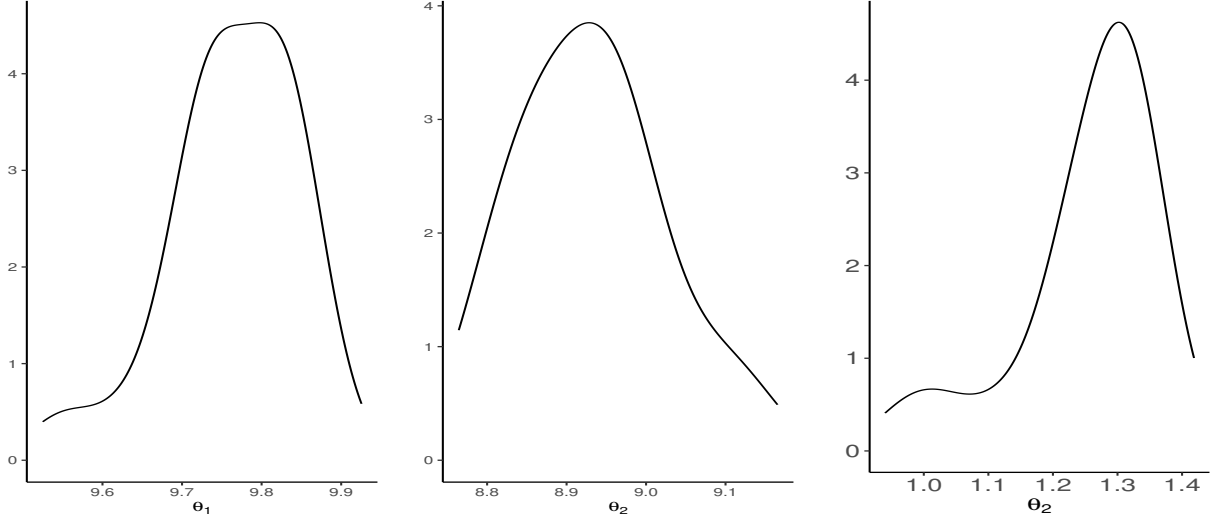


Figure 5: Posterior distribution of θ from multivariate PBART fit for the Schwarzschild model.

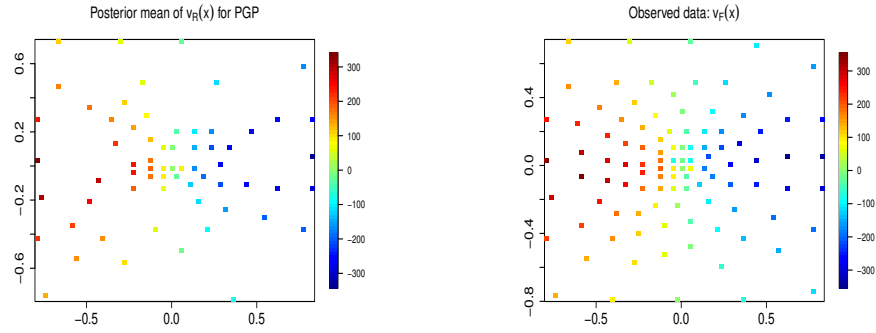


Figure 6: Posterior predictive mean of PBART is plotted for $v_R(\cdot)$ in the first panel. In the second panel, the observed values $v_F(\cdot)$ are also shown for reference.

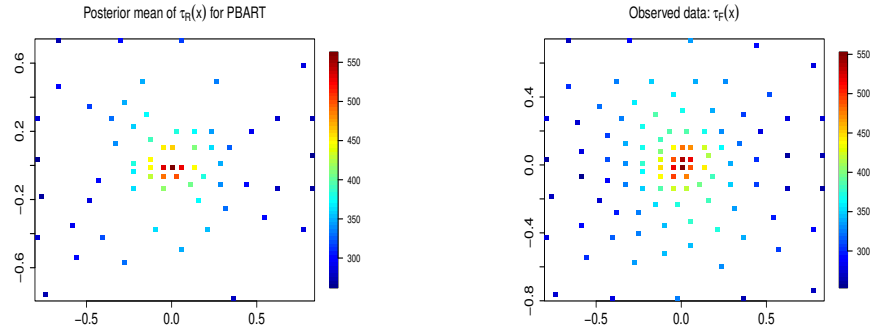


Figure 7: Posterior predictive mean of PBART is plotted for $\tau_R(\cdot)$ in the first panel. In the second panel, the observed values $\tau_F(\cdot)$ are also shown for reference.

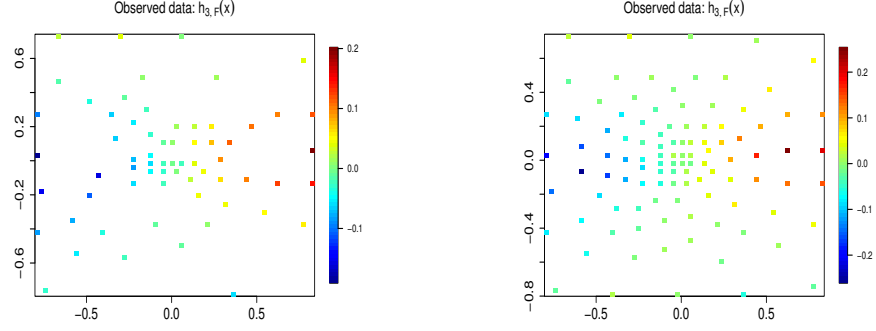


Figure 8: Posterior predictive mean of PBART is plotted for $h_{3,R}(\cdot)$ in the first panel. In the second panel, the observed values $h_{3,F}(\cdot)$ are also shown for reference.

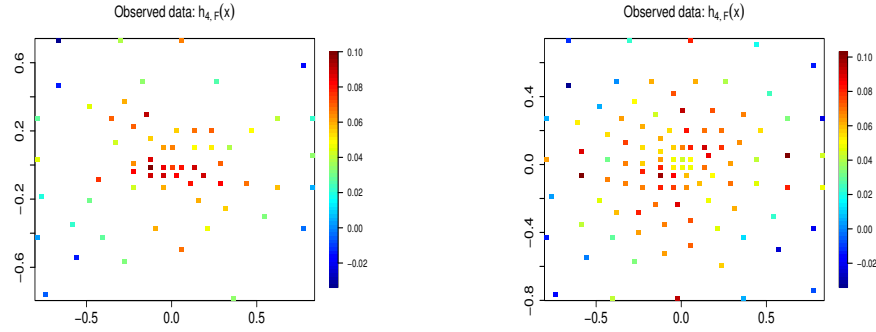


Figure 9: Posterior predictive mean of PBART is plotted for $h_{4,R}(\cdot)$ in the first panel. In the second panel, the observed values $h_{4,R}(\cdot)$ are also shown for reference.

7 Discussion

The Schwarzschild model, although computationally intensive, is an important tool in understanding the dynamics of a black hole and its host galaxy. Motivated by this application we developed a multivariate calibration method that ensures parameter identifiability under the squared error loss. The key benefits of the proposed projection posterior approach is its flexibility in accommodating user-specified prior distributions on the multivariate bias function, and the fact that such a projection is available analytically. Benefits of a multivariate analysis is demonstrated through numerical experiments and it seems to impact the analysis of Schwarzschild model positively as well. Conceptually, the projection approach can be extended to alternative loss functions that lead to different sufficiency conditions for identifiability and high-dimensional outcomes where low-rank models for the error covariance might be warranted.

References

- Bayarri, M., D. Walsh, J. Berger, J. Cafeo, G. Garcia-Donato, F. Liu, J. Palomo, R. Parthasarathy, R. Paulo, and J. Sacks (2007). Computer model validation with functional output. *Annals of Statistics* 35(5), 1874–1906.
- Bayarri, M. J., J. O. Berger, R. Paulo, J. Sacks, J. A. Cafeo, J. Cavendish, C.-H. Lin, and J. Tu (2007). A framework for validation of computer models. *Technometrics* 49(2), 138–154.
- Chakraborty, A., B. K. Mallick, R. G. Mcclarren, C. C. Kuranz, D. Bingham, M. J. Grosskopf, E. M. Rutter, H. F. Stripling, and R. P. Drake (2013). Spline-based emulators for radiative shock experiments with measurement error. *Journal of the American Statistical Association* 108(502), 411–428.
- Chipman, H. A., E. I. George, and R. E. McCulloch (2010). BART: Bayesian additive regression trees. *The Annals of Applied Statistics* 4(1), 266–298.
- Denison, D. G., B. K. Mallick, and A. F. Smith (1998). Bayesian mars. *Statistics and Computing* 8(4), 337–346.
- Forest, C. E., B. Sansó, and D. Zantedeschi (2008). Inferring climate system properties using a computer model. *Bayesian Analysis* 3(1), 1–37.
- Friedman, J. H. (1991). Multivariate adaptive regression splines. *The annals of statistics* 19(1), 1–67.

- Gattiker, J., D. Higdon, S. Keller-McNulty, M. McKay, L. Moore, and B. Williams (2006). Combining experimental data and computer simulations, with an application to flyer plate experiments. *Bayesian Analysis* 1(4), 765–792.
- Gneiting, T. and A. E. Raftery (2007). Strictly proper scoring rules, prediction, and estimation. *Journal of the American statistical Association* 102(477), 359–378.
- Haario, H., E. Saksman, J. Tamminen, et al. (2001). An adaptive Metropolis algorithm. *Bernoulli* 7(2), 223–242.
- Higdon, D., J. Gattiker, B. Williams, and M. Rightley (2008). Computer model calibration using high-dimensional output. *Journal of the American Statistical Association* 103(482), 570–583.
- Kennedy, M. C. and A. O’Hagan (2001). Bayesian calibration of computer models. *Journal of the Royal Statistical Society: Series B (Statistical Methodology)* 63(3), 425–464.
- Kormendy, J. and L. C. Ho (2013, August). Coevolution (Or Not) of Supermassive Black Holes and Host Galaxies. *Annual Review of Astronomy and Astrophysics* 51(1), 511–653.
- Linero, A. R. and Y. Yang (2018). Bayesian regression tree ensembles that adapt to smoothness and sparsity. *Journal of the Royal Statistical Society: Series B (Statistical Methodology)* 80(5), 1087–1110.
- Marmin, S. and M. Filippone (2022). Deep gaussian processes for calibration of computer models. *Bayesian Analysis* 1(1), 1–30.
- McConnell, N. J. and C.-P. Ma (2013, February). Revisiting the Scaling Relations of Black Hole Masses and Host Galaxy Properties. *The Astrophysical Journal* 764(2), 184.
- Mehrgan, K., J. Thomas, R. Saglia, X. Mazzalay, P. Erwin, R. Bender, M. Kluge, and M. Fabricius (2019, December). A 40 Billion Solar-mass Black Hole in the Extreme Core of Holm 15A, the Central Galaxy of Abell 85. *The Astrophysical Journal* 887(2), 195.
- Neal, R. M. (2012). *Bayesian learning for neural networks*, Volume 118. Springer Science & Business Media.
- Plumlee, M. (2017). Bayesian calibration of inexact computer models. *Journal of the American Statistical Association* 112(519), 1274–1285.
- Plumlee, M. and V. R. Joseph (2018). Orthogonal gaussian process models. *Statistica Sinica*, 601–619.

- Pollard, D. and P. Radchenko (2006). Nonlinear least-squares estimation. *Journal of Multivariate Analysis* 97(2), 548–562.
- Pratola, M. T. and D. M. Higdon (2016). Bayesian additive regression tree calibration of complex high-dimensional computer models. *Technometrics* 58(2), 166–179.
- Quenneville, M. E., C. M. Liepold, and C.-P. Ma (2021). Dynamical modeling of galaxies and supermassive black holes: Axisymmetry in triaxial schwarzschild orbit superposition models. *The Astrophysical Journal Supplement Series* 254(2), 25.
- Rasmussen, C. E. and C. K. I. Williams (2005). *Gaussian Processes for Machine Learning (Adaptive Computation and Machine Learning)*. The MIT Press.
- Ročková, V. and S. van der Pas (2020). Posterior concentration for bayesian regression trees and forests. *The Annals of Statistics* 48(4), 2108–2131.
- Sacks, J., W. J. Welch, T. J. Mitchell, and H. P. Wynn (1989). Design and analysis of computer experiments. *Statistical science* 4(4), 409–423.
- Saglia, R. P., M. Opitsch, P. Erwin, J. Thomas, A. Beifiori, M. Fabricius, X. Mazzalay, N. Nowak, S. P. Rusli, and R. Bender (2016, February). The SINFONI Black Hole Survey: The Black Hole Fundamental Plane Revisited and the Paths of (Co)evolution of Supermassive Black Holes and Bulges. *The Astrophysical Journal* 818(1), 47.
- Salter, J. M., D. B. Williamson, J. Scinocca, and V. Kharin (2018). Uncertainty quantification for spatio-temporal computer models with calibration-optimal bases. *arXiv preprint arXiv:1801.08184* 12.
- Santner, T. J., B. J. Williams, and W. I. Notz (2003). *The Design and Analysis of Computer Experiments*. Springer series in statistics. Springer.
- Schwarzschild, M. (1979). A numerical model for a triaxial stellar system in dynamical equilibrium. *The Astrophysical Journal* 232, 236–247.
- Sen, D., S. Patra, and D. Dunson (2018). Constrained inference through posterior projections. *arXiv preprint arXiv:1812.05741*.
- Tsiatis, A. A. (2006). *Semiparametric theory and missing data*, Volume 4. Springer.
- Tuo, R. and C. J. Wu (2015). Efficient calibration for imperfect computer models. *Annals of Statistics* 43(6), 2331–2352.

- Tuo, R. and C. J. Wu (2016). A theoretical framework for calibration in computer models: parametrization, estimation and convergence properties. *SIAM/ASA Journal on Uncertainty Quantification* 4(1), 767–795.
- van den Bosch, R., G. Van De Ven, E. Verolme, M. Cappellari, and P. De Zeeuw (2008). Triaxial orbit based galaxy models with an application to the (apparent) decoupled core galaxy ngc 4365. *Monthly Notices of the Royal Astronomical Society* 385(2), 647–666.
- Xie, F. and Y. Xu (2021). Bayesian projected calibration of computer models. *Journal of the American Statistical Association* 116(536), 1965–1982.
- Yang, Y., A. Bhattacharya, and D. Pati (2017). Frequentist convergence and sup-norm convergence rate in gaussian process regression. *arxiv preprint arXiv:1708.04753*.

A Proofs

A.1 Proof of Proposition 3.2

Proof. We first characterize θ in terms of the expected loss. Recall that for $Q = I_q$, $\theta = \arg \min_{t \in \Theta} \int_x \sum_{k=1}^q \{y_{R,k}(x) - f_k(x, t)\}^2 dx$. For any fixed $t \in \Theta$, let $e(x) = \{y^F(x) - f(x, t)\}$, then

$$\begin{aligned} E_P\{e(x)^T e(x)\} &= (\text{Vol}(\mathcal{X}))^{-1} \int_x \left[\sum_{k=1}^q E_{P_{y|x}} \{e_k^2(x)\} \right] dx \\ &= (\text{Vol}(\mathcal{X}))^{-1} \int_x \sum_{k=1}^q E_{P_{y|x}} \{y_{F,k} - y_{R,k}(x)\}^2 dx + (\text{Vol}(\mathcal{X}))^{-1} \int_x \sum_{k=1}^q \{y_{R,k}(x) - f_k(x, t)\}^2 dx \\ &= \text{tr}(\Sigma_F) + (\text{Vol}(\mathcal{X}))^{-1} \int_x e(x)^T e(x) dx, \end{aligned}$$

where $\text{tr}(A)$ denotes the trace of a matrix A . Hence, θ can be seen as

$$\arg \min_{t \in \Theta} \int_x \sum_{k=1}^q \{y_{R,k}(x) - f_k(x, t)\}^2 dx = \arg \min_{t \in \Theta} E_P[e(x)^T e(x)].$$

Now define $Q_{n,k}(t) = n^{-1} \sum_{i=1}^n \{y_{F,k}(x_i) - f_k(x_i, t)\}^2$ and $Q_n(t) = q^{-1} \sum_{k=1}^q Q_{n,k}(t)$ which is simply $E_{P_n}[e(x)^T e(x)]$ where P_n is the corresponding joint empirical measure. Invoking Theorem 3 of [Pollard and Radchenko \(2006\)](#) and the compactness of Θ , we get that $\sup_f |Q_n(t) - E_P(Q_n(t))| \xrightarrow{P} 0$ which implies that $\theta_n^* \xrightarrow{P} \theta$. \square

A.2 Proof of Lemma 3.3

Proof. The projection operator is the solution to the optimization problem

$$\min \|b_\theta - b_\theta^*\|_{L_q^2} \quad \text{subject to} \quad \sum_{k=1}^q \langle g_{j,k}, b_{\theta,k}^* \rangle = 0, \quad j = 1, \dots, p.$$

Hence, the Lagrangian dual of the optimization problem is

$$\min \sum_{k=1}^q \|b_{\theta,k} - b_{\theta,k}^*\|_L^2 + \sum_{j=1}^p \lambda_j \left[\sum_{k=1}^q \langle g_{j,k}, b_{\theta,k}^* \rangle \right].$$

Solving for $b_{\theta,k}^*$ gives $b_{\theta,k}^* = b_{\theta,k} + \sum_{j=1}^p \lambda_j g_{j,k}$. Thus, $\|b_{\theta,k} - b_{\theta,k}^*\|_{L_q^2} = \lambda^\top (\sum_{k=1}^q Q_k) \lambda$ where $\lambda = (\lambda_1, \dots, \lambda_p)^\top$ and $Q_k^{p \times p}$ is a matrix with (j, j') -th element $\langle g_{j,k}, g_{j',k} \rangle$. Also, $\sum_{k=1}^q \langle g_{j,k}, b_{\theta,k}^* \rangle = \sum_{k=1}^q \langle g_{j,k}, b_{\theta,k} \rangle + \sum_{j'=1}^p \lambda_{j'} Q_{k,jj'}$. This implies that $Q\lambda = -\eta$ where $\eta \in \mathbb{R}^{p \times 1}$ with $\eta_j = \sum_{k=1}^q \langle g_{j,k}, b_{\theta,k} \rangle$ which proves the result. \square

Supplementary materials for “Orthogonal calibration via posterior projections with applications to the Schwarzschild model”

S.1 Finite-dimensional projection

When the central focus of analysis is assessing uncertainty in θ , and $\Pi(b_k)$ is a Gaussian process, then the projection posterior approach can be implemented within a finite dimensional setting by ensuring $\sum_{k=1}^q \mathbf{b}_k^\top \mathbf{g}_{j,k} = 0$ where $\mathbf{b}_k = (b_k(x_1), \dots, b_k(x_n))^\top$ and $\mathbf{g}_{j,k} = (g_{j,k}(x_1), \dots, g_{j,k}(x_n))$. This is a consequence of posteriors of \mathbf{b}_k being Gaussian under a Gaussian process prior and projections of multivariate Gaussian random vectors to linear subspaces. For example, suppose $X^{d \times 1} \sim N(\mu, \Sigma)$ and consider the set $S = \{x : A^\top x = 0\} \subset \mathbb{R}^n$ where $A^{d \times p}$ is matrix of rank p . The conditional distribution of $X \mid X \in S$ is again a multivariate Gaussian with mean $\mu - \Sigma A^\top (A \Sigma A^\top)^{-1} A \mu$ and covariance matrix $\Sigma - \Sigma A^\top (A \Sigma A^\top)^{-1} A \Sigma$. Next, define the following projection for any $x \in \mathbb{R}^d$

$$P_S(x) = \Sigma^{1/2} \arg \min_{y \in S} \|y - \Sigma^{-1/2} x\|. \quad (\text{S.1})$$

Standard linear algebra yields that $P_S(x)$ has the form $\Sigma^{1/2}(I - P_A)\Sigma^{-1/2}y$ where $P_A = A(A^\top A)^{-1}A^\top$ is the projection matrix of A . This leads to the following interpretation of the multivariate Gaussian distribution conditional on linear equality constraints.

Proposition S.1.1. *Suppose $X \sim N(\mu, \Sigma)$ and consider the set $S = \{x : A^\top x = 0\} \subset \mathbb{R}^d$ where $A^{d \times p}$ is matrix of rank p . Then the random variable*

$$P_S(X) \sim N(\mu - \Sigma A^\top (A \Sigma A^\top)^{-1} A \mu, \Sigma - \Sigma A^\top (A \Sigma A^\top)^{-1} A \Sigma).$$

Proof. We have

$$\begin{aligned} \text{Cov}(X \mid X \in S) &= \Sigma - \Sigma A^\top (A \Sigma A^\top)^{-1} A \Sigma \\ &= \Sigma^{1/2} (I - \Sigma^{1/2} A^\top (A \Sigma A^\top)^{-1} A \Sigma^{1/2}) \Sigma^{1/2} \\ &= \Sigma^{1/2} (I - P_B) \Sigma^{1/2} = \Sigma^{1/2} (I - P_B)^2 \Sigma^{1/2} = \text{Cov}(P_S(X)), \end{aligned}$$

where $B = A \Sigma^{1/2}$ and $P_B = P_A$ since A is full rank and Σ is non-singular by assumption. A similar analysis shows that the mean also agrees. \square

The proof is provided in the appendix. We illustrate this within the orthogonal calibration context. For the sake of simplicity, consider $q = 1$. We set $A^{n \times p} = (a_1, \dots, a_p)$ where

$a_j = (g_j(x_1, \tilde{\theta}), \dots, g_j(x_n, \tilde{\theta}))^\top$. Let $b = (b(x_1), \dots, b(x_n))^\top$ denote the vector of bias function evaluated at x_1, \dots, x_n . Then the finite-dimensional analogue of the orthogonality condition is $A^\top b = 0$. When $b_{\tilde{\theta}}(\cdot)$ is endowed with a zero mean Gaussian process prior with covariance kernel $C(\cdot, \cdot)$, then *a priori* the vector $b_{\tilde{\theta}} \sim N(0, K)$ with $K_{ij} = C(x_i, x_j)$, $1 \leq i, j \leq n$. Also, $b_{\tilde{\theta}} \mid \theta, y^{(n)} \sim N((K + \sigma_F^2)^{-1} z^{(n)}, (K + \sigma_F^2)^{-1})$ where $z^{(n)} = (y(x_1) - f(x_1, \theta), \dots, y(x_n) - f(x_n, \theta))^\top$. Using Proposition S.1.1, we can then obtain b^* . Hence, for Gaussian process priors, only the second step in Algorithm 1 from the main draft will change under the finite-dimensional projection setup.

We now demonstrate how the finite-dimensional projection can be executed when $b_{\tilde{\theta}}$ is specified a non-Gaussian process prior. Here the posterior of \mathbf{b}_k is also non-Gaussian. Suppose the prior is parameterized by η . For instance, with a BART prior, η contains the trees and leaf node parameters. A prior on $b_{\tilde{\theta}}$ is specified by a prior distribution on η which then produces a full conditional distribution of $\eta \mid \theta, y^{(n)}$. A posterior sample of $b_{\tilde{\theta}} \in \mathbb{R}^n$ can be drawn by sampling from $\eta \mid \theta, y^{(n)}$. For many priors, the joint distribution can be well approximated by a multivariate Gaussian with some mean and covariance (β, Φ) (Yang et al., 2017). To find the approximating mean and covariance, we simply draw M independent draws of $b_{\tilde{\theta}}$ by sampling $\{\eta_1, \dots, \eta_M\}$ independently from $\eta \mid \theta, y^{(n)}$ and set $\beta = M^{-1} \sum_{m=1}^M b_{\tilde{\theta},m}$ and $\Phi = (M-1)^{-1} \sum_{m=1}^M (b_{\tilde{\theta},m} - \beta)(b_{\tilde{\theta},m} - \beta)^\top$ where $b_{\tilde{\theta},m}$ is the draw of $b_{\tilde{\theta}}$ corresponding to η_m , $m = 1, \dots, M$. We note here, that M can be made arbitrarily large compared to the dimension n of $b_{\tilde{\theta}}$ so that the sample mean and covariance provide reasonable approximations to their population counterparts. This technique is summarized in the following algorithm.

Algorithm 2: Projection sampler 2: non-GP priors

1. Sample M independent copies of parameters $\eta \mid \theta, y^{(n)}$ and consider the corresponding draws of $b_{\tilde{\theta}}$ as $\{b_{\tilde{\theta},1}, \dots, b_{\tilde{\theta},M}\}$.
 2. Compute the quantities $\beta = M^{-1} \sum_{m=1}^M b_{\tilde{\theta},m}$ and $\Phi = (M-1)^{-1} \sum_{m=1}^M (b_{\tilde{\theta},m} - \beta)(b_{\tilde{\theta},m} - \beta)^\top$.
 2. Set the projection as $b_{\tilde{\theta}}^* = \Phi^{1/2}(I - P_G)\Phi^{-1/2}b_{\tilde{\theta}}$.
 3. Update $\theta \sim \Pi(\theta \mid b_{\tilde{\theta}}^*, y^{(n)})$.
-

Clearly, for non-Gaussian priors for b_k , the finite-dimensional projection approach is computationally much more expensive. However, if the prior is a GP, this approach is relatively less expensive to implement and yields similar results to the functional projection approach described in the main draft.